Letter

Anticollinear order and degeneracy lifting in square lattice antiferromagnet $LaSrCrO_4$

Jing Zhou,[1,2] Guy Quirion,[3] Jeffrey A. Quilliam,[4] Huibo Cao,[5] Feng Ye,[5] Matthew B. Stone,[5] Qing Huang,[6] Haidong Zhou,[6] Jinguang Cheng,[1] Xiaojian Bai,[7,*] Martin Mourigal,[7] Yuan Wan,[1,2,8,†] and Zhiling Dun[1,7,‡]

[1]*Institute of Physics, Chinese Academy of Sciences, Beijing 100190, China*
[2]*University of the Chinese Academy of Sciences, Beijing 100049, China*
[3]*Department of Physics and Physical Oceanography, Memorial University of Newfoundland, St. John's, Canada A1B 3X7*
[4]*Institute Quantique, Département de Physique, and RQMP, Université de Sherbrooke, Sherbrooke, Québec, Canada J1K 2R1*
[5]*Neutron Scattering Division, Oak Ridge National Laboratory, Oak Ridge, Tennessee 37831, USA*
[6]*Department of Physics and Astronomy, University of Tennessee, Knoxville, Tennessee 37996, USA*
[7]*School of Physics, Georgia Institute of Technology, Atlanta, Georgia 30332, USA*
[8]*Songshan Lake Materials Laboratory, Dongguan, Guangdong 523808, China*

(Received 11 March 2022; accepted 12 May 2022; published 23 May 2022)

We report the static and dynamic magnetic properties of $LaSrCrO_4$, a seemingly canonical spin-3/2 square-lattice antiferromagnet that exhibits frustration between magnetic layers—owing to their AB stacking—and offers a rare testbed to investigate accidental-degeneracy lifting in magnetism. Neutron diffraction experiments on single-crystal samples uncover a remarkable anticollinear magnetic order below $T_N = 170$ K characterized by a Néel arrangement of the spins within each layer and an orthogonal arrangement between adjacent layers. To understand the origin of this unusual magnetic structure, we analyze the spin-wave excitation spectrum by means of inelastic neutron scattering and bulk measurements. A spectral gap of 0.5 meV, along with a spin-flop transition at 3.2 T, reflect the energy scale associated with the degeneracy-lifting. A minimal model to explain these observations requires both a positive biquadratic interlayer exchange and dipolar interactions, both of which are on the order of 10^{-4} meV, only a few parts per million of the dominant exchange interaction $J_1 \approx 11$ meV. These results provide direct evidence for the selection of a noncollinear magnetic structure by the combined effect of two distinct degeneracy lifting interactions.

DOI: 10.1103/PhysRevB.105.L180411

I. INTRODUCTION

The emergence of accidental ground-state degeneracy and its lifting are central to our understanding of frustrated magnetism [1–3]. The interplay between exchange interactions and lattice geometry often result in a family of accidentally degenerate ground states that are unrelated by symmetry. The degeneracy is then lifted either by subleading interactions, e.g., magnetic dipolar interaction [4–8], magnetoelastic coupling [9,10], etc. or by fluctuations that normally work against ordering, e.g., quenched disorder, thermal or quantum fluctuations, through the "order by disorder (ObD)" mechanism [11–17]. The diverse degeneracy lifting mechanisms can stabilize a host of magnetic orders in materials with similar structures and chemical compositions [18,19], and their competition offers flexible tunablity in and out of equilibrium [20,21]. Yet experimentally revealing the degeneracy lifting mechanism is a challenging task due to the minuscule energy scales, sometimes in one part per million of the dominant exchange interaction associated with these subleading interactions and/or the ObD effects [22].

The quasi-two-dimensional (2D) square lattice Heisenberg antiferromagnet with AB stacking is a prominent model system to illustrate the diverse degeneracy lifting mechanisms and the wealth of resulting magnetic orders[15,23–25]. The antiferromagnetic intralayer exchange interaction stabilizes a 2D Néel order in each layer. However, the interlayer exchange interactions are frustrated due to the AB stacking. Consequently, the Néel vectors in two adjacent layers remain decoupled at the mean-field level, thereby giving rise to a continuous manifold of accidentally degenerate ground states, which can then be selected by various mechanisms. In particular, the thermal and quantum fluctuations stabilize the collinear arrangement of Néel vectors through the ObD mechanism, whereas the quenched disorder favors anticollinear orders where the Néel vectors are orthogonal [15].

Experimentally, such interlayer frustration exists in a large family of transition metal oxides with a layered perovskite structure of the K_2NiF_4 type [space group $I4/mmm$, Fig. 2(a)] and easy-plane single-ion anisotropy. Focusing on simple systems without secondary magnetic lattices or electron/hole doping, including La_2MO_4 (M = Cu [26], Ni [27,28], Co [29–31]), $LaSrFeO_4$ [32], and $Sr_2CuO_2Cl_2$ [33], all of these compounds exhibit collinear orders without exception [Figs. 1(b) and 1(c)]. In La_2MO_4 (M = Cu, Ni, Co),

*Present address: Neutron Scattering Division, Oak Ridge National Laboratory, Oak Ridge, TN 37831, USA.
†yuan.wan@iphy.ac.cn
‡dun@iphy.ac.cn

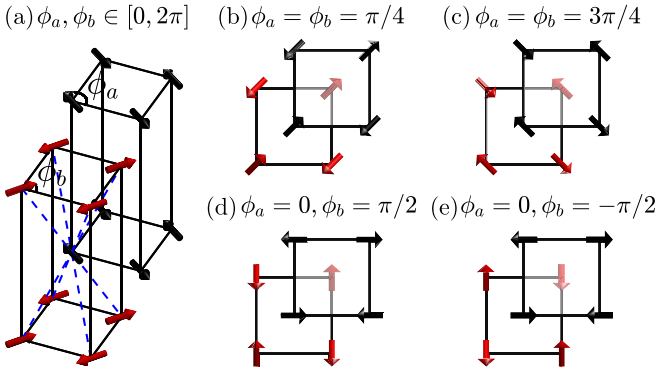

FIG. 1. (a) The quasi-2D square lattice antiferromagnet with AB stacking comprises of two sublattices (dubbed A and B), each hosting a 3D Néel order. The two Néel vectors are decoupled at the mean-field level owing to the frustrated interlayer coupling. An easy-plane single-ion anisotropy forces the Néel vectors to be in the crystallographic *ab* plane, which are then parametrized by their respective azimuthal angles (ϕ_a, ϕ_b). (b) Collinear spin structure with $\phi_a = \phi_b = \frac{\pi}{4}$ observed in La_2CuO_4 [26], $Sr_2CuO_2Cl_2$ [33], $LaSrFeO_4$ [32], and La_2CoO_4 in the orthorhombic phase [29]. (c) Collinear spin structure with $\phi_a = \phi_b = \frac{3\pi}{4}$ for La_2NiO_4 [27] and possibly La_2CoO_4 in the low-temperature tetragonal phase [29,30]. (d) Anticollinear state with $\phi_a = 0$, $\phi_b = \frac{\pi}{2}$, for $LaSrCrO_4$ reported in this work. (e) The other symmetry-inequivalent anticollinear order with $\phi_a = 0$, $\phi_b = -\frac{\pi}{2}$.

the orthorhombic lattice distortion lifts the degeneracy and stabilizes the collinear order [27,29,34]. In $LaSrFeO_4$ and $Sr_2CuO_2Cl_2$, the lattice distortion is absent; the degeneracy lifting mechanism is less clear though thermal or quantum fluctuations are likely responsible [15,25].

In this work, we investigate a much less characterized member of this material family, $LaSrCrO_4$ (LSCrO) [35–37]. Using neutron-scattering measurements on a single-crystal sample, we reveal a striking *anticollinear* magnetic ground state [Fig. 1(d)] that is distinct from all the compounds mentioned above. Combining theoretical analysis with various experimental measurements, we show that the magnetic dipolar interaction and the biquadratic spin-exchange interaction, both on the order of 10^{-5} (10 ppm) of the main exchange interaction J_1, are responsible for lifting the degeneracy and stabilizing the anticollinear state in this material. Our results thus establish LSCrO as a rare example where the degeneracy lifting interactions with minuscule energy scales can be exposed unambiguously.

II. ANTICOLLINEAR ORDER

We grow for the first time centimeter-sized single crystals of LSCrO via the floating zone technique [40]. X-ray and neutron diffraction measurements confirm that it crystallizes in the tetragonal space group $I4/mmm$ at room temperature with lattice constants $a = b = 3.853(6)$ Å, $c = 12.475(4)$ Å [Fig. 2(a)], consistent with previous reports [35,37]. By using Rietveld refinement of the nuclear Bragg peaks measured at various temperatures, we found no structural phase transitions down to 4 K. Similar to other quasi-2D systems [41], the magnetic ordering in LSCrO occurs in two steps. At temperatures

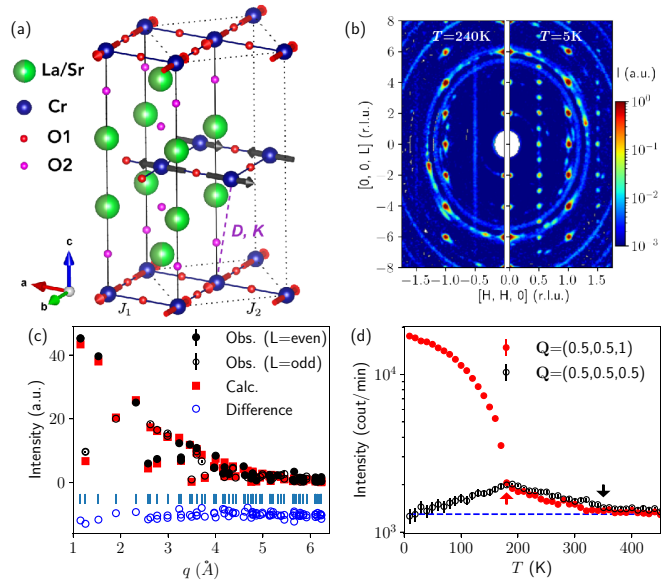

FIG. 2. (a) Nuclear and magnetic unit cells (represented by solid and dotted lines) of LSCrO. Colored spheres present different atoms and red/black arrows presents Cr^{3+} spins that are orthogonal between adjacent layers. Spin interactions J_1, J_2, D, K in Eqs. (1) and (2) are labeled for selective Cr-Cr bonds. (b) Elastic neutron-scattering patterns in the (HHL) plane, measured on SEQUOIA (Spallation Neutron Source, Oak Ridge National Laboratory, Ref. [38]) at $T = 240$ and 5 K, respectively. Intensities are integrated within ±0.1 reciprocal-lattice unit (r.l.u.) in the [KK̄0] direction. (c) Rietveld refinement of the magnetic reflections collected on HB3a (High Flux Isotope Reactor, ORNL, Ref. [39]) at 4 K based on the magnetic structure shown in (a). (d) Temperature dependence of the magnetic diffuse scattering intensity at $\mathbf{Q} = (0.5, 0.5, 0.5)$ and magnetic Bragg peak intensity at $\mathbf{Q} = (0.5, 0.5, 1)$. The onset temperatures and 2D and 3D magnetic ordering are indicated by the arrows.

below 350 K, short-ranged 2D Néel order develops gradually, evidenced by the increasing magnetic scattering intensities at the M point of the square lattice Brillouin zone, which are diffuse along the L direction [Figs. 2(b) and 2(d)].

Below $T_N = 170$ K, the diffuse scattering quickly concentrates into sharp magnetic Bragg peaks at wave-vectors $\mathbf{Q} = (H + \frac{1}{2}, K + \frac{1}{2}, L)$ in reciprocal space [Fig. 2(b)], pinpointing a 3D ordering of Cr^{3+} spins. Interestingly, magnetic Bragg peaks are observed at $\mathbf{Q}$ with *both* even and odd L [Figs. 2(b) and 2(c)]. This observation cannot be explained by the 3D Néel order with a single ordering wave vector, where the magnetic structure factor would be extinct at either even or odd L [40,42]. In other words, the spins in adjacent planes cannot be strictly collinear. A Rietveld refinement of magnetic Bragg peak intensities collected at 4 K indicates that the magnetic structure is best fit by a 2-k model [$k_1 = (1/2, 1/2, 0)$ and $k_2 = (1/2, -1/2, 0)$] with the ordered moment of $2.25(2)\mu_B/Cr^{3+}$, characterized by the magnetic space group P_C4_2/ncm [43]. The resulting magnetic structure is shown in Fig. 2(a), which is identical to the anticollinear structure shown in Fig. 1(d).

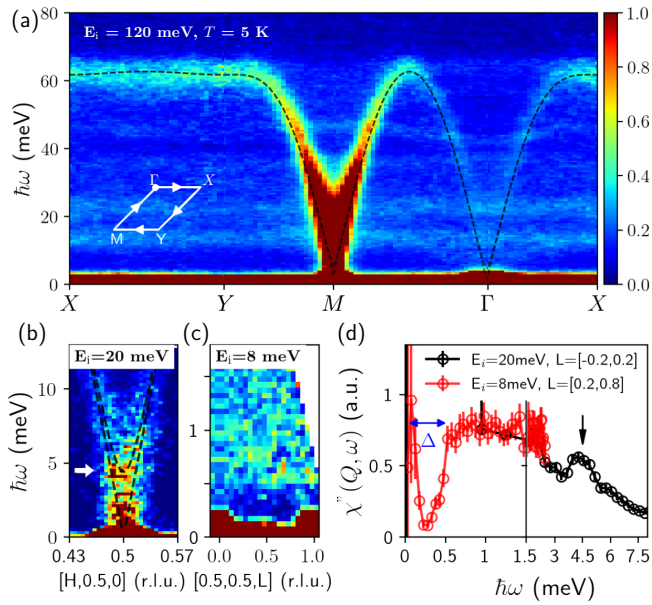

FIG. 3. (a) Spin-wave excitations along high-symmetry directions in the 2D Brillouin zone (inset) measured on SEQUOIA using $E_i = 120$ meV. Data are integrated within $H, K = \pm 0.2$ and $L = \pm 8$ r.l.u. The flat modes near 10 and 20 meV are optical phonons at high L values. (b) Dispersion along H near the M-point of the 2D Brillouin zone measured at $E_i = 20$ meV. Data integration range is $H(K) = \pm 0.03$ and $L = \pm 0.15$ r.l.u. Dashed lines in (a) (b) represent best fit to Eq. 1 from LSWT. (c) Dispersion along $[0.5, 0.5, L]$ measured at $E_i = 8$ meV. Data integration range is $H, K = \pm 0.02$ r.l.u. (d) Dynamic magnetic susceptibility at the M point, obtained by integrating the data in (c). All data shown in this figure are collected at $T = 5$ K and symmetrized according to the D_{4h} point group symmetry of the Cr^{3+} site.

III. SPIN-WAVE EXCITATIONS

We investigate the low-temperature magnetic excitation spectrum of LSCrO using time-of-flight neutron spectroscopy with various neutron incident energies (E_i) [40]. Figure 3(a) shows the overall energy-momentum dependence of the measured dynamic structure factor $S(q, \omega)$ along the high-symmetry directions of the 2D Brillouin zone, where the scattering intensities are integrated along the L direction. An intense and dispersive spin-wave band emanates from the M point. Its intensities gradually diminish when moving to the Γ point. The spin-wave shows almost no dispersion from the X point to the Y point, suggesting that further-neighbor exchange couplings [44] and quantum anomaly effects [45] are small.

Using a lower incident energy, $E_i = 20$ meV, and therefore better energy resolution, we identify an energy gap of 4.5(1) meV in the M-point spectrum [indicated by arrows in Figs. 3(b) and 3(d)]. We attribute this gap to the weak, easy-plane single-ion anisotropy of the Cr^{3+} moments.

Given the large spin carried by the Cr^{3+} ions [electron configuration t_{2g}^3, $S = 3/2$], we expect that the observed spectrum can be understood in terms of the linear spin-wave theory (LSWT). We find that the following minimal model Hamiltonian, which includes the first- (J_1) and the second-neighbor (J_2) exchange interactions, as well as an easy-plane single-ion anisotropy (A), can well describe the in-plane dispersion of the spin wave within the LSWT framework,

$$\mathcal{H}_0 = J_1 \sum_{\langle ij \rangle_1} \mathbf{S}_i \cdot \mathbf{S}_j + J_2 \sum_{\langle ij \rangle_2} \mathbf{S}_i \cdot \mathbf{S}_j + A \sum_i \left(S_i^z\right)^2, \quad (1)$$

where the summation $\langle ij \rangle_n$ runs over n-th neighbor spin pairs. We attain the best fit [dashed black lines in Figs. 3(a) and 3(b)] with $J_1 = 10.6(1)$ meV, $J_2 = 0.16(6)$ meV, and $A = 0.05(1)$ meV. The energy scale of the J_1 exchange is comparable to the onset temperature for the short-ranged 2D Néel order.

Finally, we examine the low-energy dispersion along the L direction at the M point with the best energy resolution obtained at $E_i = 8$ meV [Fig. 3(c)]. Remarkably, the spectrum is gaped throughout. As the gaps do not show discernible L dependence, we conclude that the interlayer couplings between Cr^{3+} spins of adjacent layers are smaller than the instrument resolution [>0.1 meV]. By integrating L in Fig. 3(c) and avoiding regions where there is inelastic leakage from magnetic Bragg peaks, we obtain the energy dependence of dynamic susceptibility $\chi''(\mathbf{Q}, \omega)$, which clearly reveals a second, much smaller gap $\Delta \approx 0.5(1)$ meV [Fig. 3(d)].

The weak interlayer coupling is expected given the relative low 3D ordering temperature, $k_B T_N / [J_1 S(S+1)] = 0.391$. As a crude estimate, we neglect the small easy-plane anisotropy and utilize the published ordering temperatures of the quasi-2D Heisenberg model as determined by quantum Monte Carlo simulations [46,47]. We estimate the interlayer coupling is in the range of 10^{-6} to 10^{-3} meV [40].

IV. INTERLAYER COUPLINGS

While the minimal model Eq. (1) can produce the in-plane dispersion of the spin wave, it is silent on the origin of the 3D magnetic structure. We now discuss the interlayer couplings that can stabilize the anticollinear state of LSCrO.

To set the stage, we determine the symmetry-allowed couplings between the Néel vectors associated with the two sublattices. The single-ion anisotropy forces the Néel vectors to lie in the plane. We parametrize the orientation of the Néel vector in the sublattice A/B by the azimuthal angle ϕ_a/ϕ_b, respectively [Fig. 1(a)]. The interaction energy can be expanded as Fourier series of $\phi_{a,b}$. Up to the fourth-order harmonics, our symmetry analysis yields three algebraically independent coupling terms [40]: $-\sin(\phi_a + \phi_b)$, $-\cos(4\phi_a) - \cos(4\phi_b)$, and $\cos(2\phi_a - 2\phi_b)$. The signs at the front are needed to energetically favor the anticollinear state, i.e., $\phi_a = 0$, $\phi_b = \pi/2$ (and symmetry-related configurations). Each term admits a physical interpretation: The first term arises from the magnetic (pseudo) dipolar interaction; the second describes an in-plane, fourfold symmetric single-ion anisotropy; the last comes from the biquadratic exchange interaction.

Stabilizing the anticollinear order found in LSCrO requires the combination of either (a) dipolar interaction and biquadratic exchange or (b) dipolar interaction and single-ion anisotropy. Note that the combination of the biquadratic exchange and the single-ion anisotropy does not fully lift the accidental degeneracy—it admits another,

symmetry-inequivalent anticollinear state $\phi_a = 0, \phi_b = -\pi/2$ [Fig. 1(e)] in addition to the state observed in LSCrO.

Among the two possible combinations, we find the first can produce the correct spin-flop transition observed in LSCrO (see below). We thus arrive at the following minimal Hamiltonian for the interlayer coupling,

$$\mathcal{H}' = \sum_{\langle ij\rangle_3} D(\mathbf{S}_i \cdot \mathbf{S}_j - 3(\mathbf{S}_i \cdot \hat{n}_{ij})(\mathbf{S}_j \cdot \hat{n}_{ij})) + K(\mathbf{S}_i \cdot \mathbf{S}_j)^2, \tag{2}$$

where the summation is over all third-neighbor pairs; $\hat{n}_{ij}$ is the unit vector pointing from site i to site j. $D > 0$ and $K > 0$ are strength of the dipolar and biqudratic couplings, respectively.

V. SPIN-FLOP TRANSITIONS

We now turn to the experimental test of the model Eq. (2). A sensitive diagnostic for the interlayer coupling is the spin-flop transition driven by a magnetic field applied within the *ab* plane. The Zeeman coupling favors the Néel vectors to be perpendicular to the field in each layer. When the field is sufficiently strong, this effect can overcome the dipolar/biquadratic interactions and stabilize a collinear state. The resulting evolution from an anticollinear to a collinear magnetic structure thus offers a probe of the nature and strength of the interlayer couplings.

Our theoretical analysis based on the model Eq. (2) reveals distinct magnetization processes when the field is aligned along different high-symmetry directions. Within increasing field ∥ [110], we find the angle between the Néel vectors of the two sublattices gradually increases from $\pi/2$ to π, at which point the system enters the collinear state. Meanwhile, the Néel vectors remain symmetric with respect to the field [Fig. 4(a)]. The onset field of the collinear state is given by $g\mu_B\mu_0 H_c = 16\sqrt{J_1 K S^4}$. Note this process is a crossover as opposed to a phase transition in that no symmetry is spontaneously broken.

By contrast, with the field ∥ [100], the Néel vectors are initially pinned to the anticollinear state [Fig. 4(b)]. A spin-flop transition occurs at H_{c1}, at which point the Néel vectors are no longer orthogonal and evolve toward the collinear state whereby spontaneously breaking the π-rotation symmetry with respect to [100]. The system enters the collinear state at H_{c2} although the collinear Néel vectors are not strictly orthogonal to the field. No symmetry breaking occurs at H_{c2} and thus it constitutes a crossover. With increasing field, the collinear Néel vectors continuously approach the limit where they are orthogonal to the field. $H_{c1,c2}$ are determined by

$$\frac{(g\mu_B\mu_0 H_{c1})^2}{32J_1} = \sqrt{\mathcal{K}\mathcal{D}}, \tag{3a}$$

$$\frac{(g\mu_B\mu_0 H_{c2})^2}{32J_1} = \sqrt{\frac{\mathcal{K}^2}{2} + \frac{\mathcal{K}}{2}\sqrt{\mathcal{K}^2 + 4\mathcal{D}^2}}, \tag{3b}$$

where $\mathcal{K} = 8KS^4$ and $\mathcal{D} = 12a^2DS^2/(2a^2 + c^2)$.

These predictions are confirmed experimentally by our dc magnetization measurements. The differential magnetization in [110] direction shows a maximum near 5 T, corresponding to the crossover from noncollinear to collinear states at H_c [Fig. 4(c)]. By contrast, in the field ∥ [100], we observe inflection points at 3.15(5) and 5 T [Fig. 4(d)]. We identify the inflection near 3 T as the spin-flop transition at H_{c1} and the one near 5 T as the crossover at H_{c2}. This interpretation is further supported by ultrasound velocity measurements [Fig. 4(f)]—a sensitive technique to investigate second-order magnetic phase transitions [49,50]. When the field is applied in the [100] direction, the relative speed of the transverse sound wave shows a clear minimum at 3.27 T, indicative of a phase transition, but no anomaly is found at 5 T. Meanwhile, neutron diffraction measurement with field ∥ [110] reveals a gradual increase (decrease) of magnetic Bragg peak intensities with even (odd) L values up to the highest measured magnetic field of 4 T [Fig. 4(e)], consistent with the picture of a gradual rotation of Néel vectors [Fig. 4(a)].

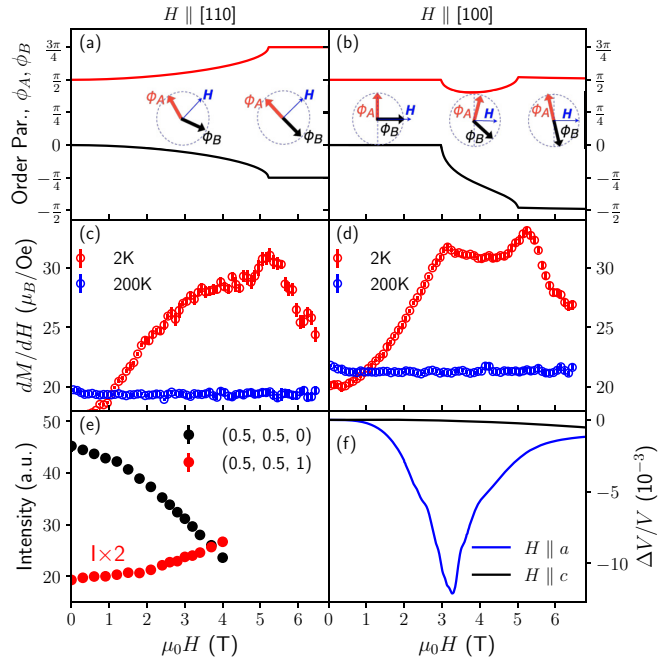

FIG. 4. (a), (b) The azimuthal angle of the Néel vectors, ϕ_a and ϕ_b, as a function of the applied magnetic field H along (a) [110] and (b) [100] directions. Inset: Configurations of the Néel vectors at selective fields. (c), (d) Differential magnetization at 2 and 200 K measured with H applied along (c) [110] and (d) [100] directions. (e) Field dependence of the magnetic Bragg peak intensities at $\mathbf{Q}$ = (0.5,0.5,0) and $\mathbf{Q}$ = (0.5,0.5,1), measured at T = 2 K on the CORELLI diffuse scattering spectrometer (SNS, ORNL, Ref. [48]) with magnetic field applied along the [1$\bar{1}$0] direction. (f) Field dependence of the relative velocity variation of the transverse mode propagating along the x axis and polarized along the y axis V_{LxPy}, measured at T = 2 K for H along the a axis (black curve) and along the c axis (blue curve).

Using the experimentally measured value of H_{c1} and H_{c2} in the [100] direction, we estimate $DS^2 \approx 1.4 \times 10^{-4}$ meV and $KS^4 \approx 1.3 \times 10^{-4}$ meV. Using these parameters, we determine the crossover field $\mu_0 H_c \approx 5$ T in the [110] direction, in agreement with the experiment. Meanwhile, the LSWT predicts that all four branches of the spin waves are gapped. The interlayer interactions open two gaps with values 0.2 and 0.6 meV. The 0.6 meV gap is consistent with the observed

spectral gap Δ [Fig. 3(d)], whereas the 0.2 meV gap is beyond the energy resolution of our measurements.

We note that the alternative model for interlayer coupling, namely, the dipolar coupling and the fourfold symmetric single-ion anisotropy, produces first-order spin-flop transitions in the [100] directions [40], which is inconsistent with the experiment.

VI. DISCUSSION

Having established the nature and strength of interlayer interactions [Eq. (2)], we now discuss their microscopic origins. The dipolar coupling D may originate from either the pseudodipolar coupling, commonly found in systems with strong spin-orbital coupling, or the magnetic dipolar interaction. Given the filled t_{2g} shell of Cr^{3+}, we do not expect significant spin-orbital coupling and thus rules out the former possibility. Note that our case is very different from isostructural compounds with a second, magnetic rare-earth sublattice, e.g., R_2CuO_4 (R = Ce, Pr, Nd) [42,51–53], which could mediate the pseudodipolar coupling [54]. Instead, we find that D is naturally attributed to the magnetic dipolar coupling. Our magnetostatic calculation yields $DS^2 \approx 2 \times 10^{-4}$ meV based on the refined moment of $2.25\mu_B/Cr^{3+}$, consistent with the estimate based on the spin-flop field. Dipolar coupling is known to be crucial for rare-earth magnets with icelike frustration [19,55–57] where the exchange interactions are small. Our work demonstrates that it can also play an important role in systems with comparatively much stronger exchange coupling.

The *positive* biquadratic exchange interaction could be generated either by higher-order virtual hopping processes in the superexchange [58] or more likely by quenched disorder due to the La/Sr mixing through the ObD mechanism [15,17]. We also note that the combination of dipolar interaction and a *negative* biquadratic exchange, produced by the thermal or quantum ObD, would stabilize a collinear order with the spins in the [110] direction, which may explain the 3D ordering in $Sr_2CuO_2Cl_2$ or $LaSrFeO_4$. This observation motivates further investigation of quenched disorder to control magnetic order in frustrated magnets or spintronic devices.

The experimental observation of the anticollinear order in LSCrO uncovers a new territory in the phase diagram of the AB-stacked square-lattice antiferromagnet. In contrast with the collinear magnetic states displayed by all related materials, the anticollinear order in LSCrO exhibits a rich and unique magnetic-field evolution stemming from interlayer effects that are merely a few parts per million of the main exchange interaction. A systematic study of the temperature-field phase diagram of LSCrO and its materials relatives is poised to reveal more surprises in this canonical family of geometrically frustrated magnets.

ACKNOWLEDGMENTS

We thank Cristian Batista and Hitesh Changlani for helpful discussions. This research used resources at the High Flux Isotope Reactor and Spallation Neutron Source, a DOE Office of Science User Facility operated by the Oak Ridge National Laboratory. The work at Institute of Physics was supported by the National Natural Science Foundation of China (Grants No. 11974396, No. 12025408, No. 11874400, and No. 12188101), the Ministry of Science and Technology (2018YFA0305700), and the Strategic Priority Research Program of the Chinese Academy of Sciences (Grant No. XDB33020300). The work of Q.H. and H.Z. at the University of Tennessee was supported by the National Science Foundation under Award No. DMR-2003117. The work of Z.L.D., X.B., and M.M. at Georgia Tech (neutron-scattering experiment and data analysis) was supported by the U.S. Department of Energy, Office of Science, Basic Energy Sciences, Materials Sciences and Engineering Division under Award No. DE-SC-0018660.

[1] A. P. Ramirez, Strongly geometrically frustrated magnets, Annu. Rev. Mater. Sci. **24**, 453 (1994).

[2] R. Moessner, Magnets with strong geometric frustration, Can. J. Phys. **79**, 1283 (2001).

[3] J. T. Chalker, Geometrically frustrated antiferromagnets: Statistical mechanics and dynamics, in *Introduction to Frustrated Magnetism: Materials, Experiments, Theory*, edited by C. Lacroix, P. Mendels, and F. Mila (Springer, Berlin, Heidelberg, 2011), pp. 3–22.

[4] R. G. Melko, B. C. den Hertog, and M. J. P. Gingras, Long-Range Order at Low Temperatures in Dipolar Spin Ice, Phys. Rev. Lett. **87**, 067203 (2001).

[5] J. P. C. Ruff, R. G. Melko, and M. J. P. Gingras, Finite-Temperature Transitions in Dipolar Spin Ice in a Large Magnetic Field, Phys. Rev. Lett. **95**, 097202 (2005).

[6] M. B. Silva Neto, L. Benfatto, V. Juricic, and C. Morais Smith, Magnetic susceptibility anisotropies in a two-dimensional quantum heisenberg antiferromagnet with Dzyaloshinskii-Moriya interactions, Phys. Rev. B **73**, 045132 (2006).

[7] G. Möller and R. Moessner, Magnetic multipole analysis of kagome and artificial spin-ice dipolar arrays, Phys. Rev. B **80**, 140409(R) (2009).

[8] G.-W. Chern, P. Mellado, and O. Tchernyshyov, Two-Stage Ordering of Spins in Dipolar Spin Ice on the Kagome Lattice, Phys. Rev. Lett. **106**, 207202 (2011).

[9] O. Tchernyshyov, R. Moessner, and S. L. Sondhi, Order by Distortion and String Modes in Pyrochlore Antiferromagnets, Phys. Rev. Lett. **88**, 067203 (2002).

[10] O. Tchernyshyov, R. Moessner, and S. L. Sondhi, Spin-Peierls phases in pyrochlore antiferromagnets, Phys. Rev. B **66**, 064403 (2002).

[11] J. R. Tessman, Magnetic anisotropy at $0°K$, Phys. Rev. **96**, 1192 (1954).

[12] J. Villain, Insulating spin glasses, Z. Phys. B: Condens. Matter Quanta **33**, 31 (1979).

[13] E. Shender, Antiferromagnetic garnets with fluctuationally interacting sublattices, Zh. Eksp. Teor. Fiz **83**, 326 (1982).

[14] H. Kawamura, Spin-wave analysis of the antiferromagnetic plane rotator model on the triangular lattice–symmetry breaking in a magnetic field, J. Phys. Soc. Jpn. **53**, 2452 (1984).

[15] C. L. Henley, Ordering Due to Disorder in a Frustrated Vector Antiferromagnet, Phys. Rev. Lett. **62**, 2056 (1989).

[16] L. Savary, K. A. Ross, B. D. Gaulin, J. P. C. Ruff, and L. Balents, Order by Quantum Disorder in $Er_2Ti_2O_7$, Phys. Rev. Lett. **109**, 167201(2012).

[17] A. I. Smirnov, T. A. Soldatov, O. A. Petrenko, A. Takata, T. Kida, M. Hagiwara, A. Y. Shapiro, and M. E. Zhitomirsky, Order by Quenched Disorder in the Model Triangular Antiferromagnet $RbFe(MoO_4)_2$, Phys. Rev. Lett. **119**, 047204 (2017).

[18] A. M. Hallas, J. Gaudet, and B. D. Gaulin, Experimental insights into ground-state selection of quantum *XY* pyrochlores, Annu. Rev. Condens. Matter Phys. **9**, 105 (2018).

[19] Z. L. Dun, J. Trinh, K. Li, M. Lee, K. W. Chen, R. Baumbach, Y. F. Hu, Y. X. Wang, E. S. Choi, B. S. Shastry, A. P. Ramirez, and H. D. Zhou, Magnetic Ground States of the Rare-Earth Tripod Kagome Lattice $Mg_2RE_3Sb_3O_{14}$ (RE = Gd, Dy, Er), Phys. Rev. Lett. **116**, 157201 (2016).

[20] Y. Wan and R. Moessner, Control of the Effective Free-Energy Landscape in a Frustrated Magnet by a Field Pulse, Phys. Rev. Lett. **119**, 167203 (2017).

[21] Y. Wan and R. Moessner, Nonequilibrium selection of magnetic order in a driven triangular XY antiferromagnet, Phys. Rev. B **98**, 184432 (2018).

[22] K. A. Ross, Y. Qiu, J. R. D. Copley, H. A. Dabkowska, and B. D. Gaulin, Order by Disorder Spin Wave Gap in the XY Pyrochlore Magnet $Er_2Ti_2O_7$, Phys. Rev. Lett. **112**, 057201 (2014).

[23] T. Yildirim, A. B. Harris, O. Entin-Wohlman, and A. Aharony, Symmetry, Spin-Orbit Interactions, and Spin Anisotropies, Phys. Rev. Lett. **73**, 2919 (1994).

[24] T. Yildirim, A. B. Harris, O. Entin-Wohlman, and A. Aharony, Spin Structures of Tetragonal Lamellar Copper Oxides, Phys. Rev. Lett. **72**, 3710 (1994).

[25] T. Yildirim, A. B. Harris, and E. F. Shender, Three-dimensional ordering in bct antiferromagnets due to quantum disorder, Phys. Rev. B **53**, 6455 (1996).

[26] D. Vaknin, S. K. Sinha, D. E. Moncton, D. C. Johnston, J. M. Newsam, C. R. Safinya, and H. E. King, Antiferromagnetism in La_2CuO_4, Phys. Rev. Lett. **58**, 2802 (1987).

[27] G. Aeppli and D. J. Buttrey, Magnetic Correlations in $La_2NiO_{4+\delta}$, Phys. Rev. Lett. **61**, 203 (1988).

[28] X. L. Wang, C. Stassis, D. C. Johnston, T. C. Leung, J. Ye, B. N. Harmon, G. H. Lander, A. J. Schultz, C. K. Loong, and J. M. Honig, Neutron-diffraction study of the antiferromagnetic form factor of La_2NiO_4, Phys. Rev. B **45**, 5645 (1992).

[29] Y. Yamada and M. Matsuda, Successive antiferromagnetic phase transitions in single-crystal La_2CoO_4, Phys. Rev. B **39**, 2336 (1989).

[30] J. Gardner, D. Paul, and B. Lcbech, Neutron diffraction study of a $La_2CoO_{4.15}$ single crystal, Phys. B: Condens. Matter **234-236**, 721 (1997).

[31] P. Babkevich, D. Prabhakaran, C. D. Frost, and A. T. Boothroyd, Magnetic spectrum of the two-dimensional antiferromagnet La_2CoO_4 studied by inelastic neutron scattering, Phys. Rev. B **82**, 184425 (2010).

[32] N. Qureshi, H. Ulbrich, Y. Sidis, A. Cousson, and M. Braden, Magnetic structure and magnon dispersion in $LaSrFeO_4$, Phys. Rev. B **87**, 054433(2013).

[33] X. L. Wang, L. L. Miller, J. Ye, C. Stassis, B. N. Harmon, D. C. Johnston, A. J. Schultz, and C. K. Loong, Antiferromagnetic form factor of $Sr_2CuO_2Cl_2$, J. Appl. Phys. **67**, 4524 (1990).

[34] A. Singh, Magnetic Dynamics in Copper-Oxide-Based Antiferromagnets: The Role of Interlayer Coupling, Phys. Rev. Lett. **64**, 2571 (1990).

[35] K. Aso, Physical properties of magnetic 2-D oxides containing Cr^{3+}, $(SrCaR)_2(Cr_xGa_{1-x})O_4$, (R=La or Sm), J. Phys. Soc. Jpn. **44**, 1083 (1978).

[36] A. Morales Sánchez, F. Fernández, R. Sáez Puche, and F. Fernández-Martín, Structural and magnetic characterization of novel stoichiometric $LnCaCrO_4$ oxides (Ln, rare earth), J. Alloys Compd. **203**, 143 (1994).

[37] T. H. Kao, H. Sakurai, T. Kolodiazhnyi, Y. Suzuki, M. Okabe, T. Asaka, K. Fukuda, S. Okubo, S. Ikeda, S. Hara, T. Sakurai, H. Ohta, and H. D. Yang, Crystal structure and physical properties of Cr and Mn oxides with $3d^3$ electronic configuration and a K_2NiF_4-type structure, J. Mater. Chem. C **3**, 3452 (2015).

[38] G. E. Granroth, A. I. Kolesnikov, T. E. Sherline, J. P. Clancy, K. A. Ross, J. P. C. Ruff, B. D. Gaulin, and S. E. Nagler, SEQUOIA: A newly operating chopper spectrometer at the SNS, J. Phys.: Conf. Ser. **251**, 012058 (2010).

[39] B. C. Chakoumakos, H. Cao, F. Ye, A. D. Stoica, M. Popovici, M. Sundaram, W. Zhou, J. S. Hicks, G. W. Lynn, and R. A. Riedel, Four-circle single-crystal neutron diffractometer at the High Flux Isotope Reactor, J. Appl. Crystallogr. **44**, 655 (2011).

[40] See Supplemental Material at http://link.aps.org/supplemental/10.1103/PhysRevB.105.L180411 for details of the experimental methods including crystal growth, susceptibility and magnetization measurements, neutron scattering measurements, and refinements of the nuclear and magnetic structure; method for estimation the energy scale of interlayer coupling; symmetry analysis for interlayer coupling; spin-wave theory and spin-flop transitions of the dipole-anisotropy and dipole-biquadratic models.

[41] D. Senff, O. Schumann, M. Benomar, M. Kriener, T. Lorenz, Y. Sidis, K. Habicht, P. Link, and M. Braden, Melting of magnetic correlations in charge-orbital ordered $La_{1/2}Sr_{3/2}MnO_4$: Competition of ferromagnetic and antiferromagnetic states, Phys. Rev. B **77**, 184413 (2008).

[42] S. Li, S. D. Wilson, D. Mandrus, B. Zhao, Y. Onose, Y. Tokura, and P. Dai, Spin-charge coupling in lightly doped $Nd_{2-x}Ce_xCuO_4$, Phys. Rev. B **71**, 054505 (2005).

[43] J. M. Perez-Mato, S. V. Gallego, E. S. Tasci, L. Elcoro, G. De La Flor, and M. I. Aroyo, Symmetry-based computational tools for magnetic crystallography, Annu. Rev. Mater. Res. **45**, 217 (2015).

[44] N. S. Headings, S. M. Hayden, R. Coldea, and T. G. Perring, Anomalous High-Energy Spin Excitations in the High-T_c Superconductor-Parent Antiferromagnet La_2CuO_4, Phys. Rev. Lett. **105**, 247001 (2010).

[45] B. Dalla Piazza, M. Mourigal, N. B. Christensen, G. J. Nilsen, P. Tregenna-Piggott, T. G. Perring, M. Enderle, D. F. McMorrow, D. A. Ivanov, and H. M. Rønnow, Fractional excitations in the square-lattice quantum antiferromagnet, Nat. Phys. **11**, 62 (2015).

[46] N. Majlis, S. Selzer, and G. C. Strinati, Dimensional crossover in the magnetic properties of highly anisotropic antiferromagnets, Phys. Rev. B **45**, 7872 (1992).

[47] C. Yasuda, S. Todo, K. Hukushima, F. Alet, M. Keller, M. Troyer, and H. Takayama, Néel Temperature of Quasi-Low-Dimensional Heisenberg Antiferromagnets, Phys. Rev. Lett. **94**, 217201(2005).

[48] F. Ye, Y. Liu, R. Whitfield, R. Osborn, and S. Rosenkranz, Implementation of cross correlation for energy discrimination on the time-of-flight spectrometer CORELLI, J. Appl. Crystallogr. **51**, 315 (2018).

[49] S. Adenwalla, S. W. Lin, Q. Z. Ran, Z. Zhao, J. B. Ketterson, J. A. Sauls, L. Taillefer, D. G. Hinks, M. Levy, and B. K. Sarma, Phase Diagram of UPt_3 from Ultrasonic Velocity Measurements, Phys. Rev. Lett. **65**, 2298 (1990).

[50] G. Quirion, M. Lapointe-Major, M. Poirier, J. A. Quilliam, Z. L. Dun, and H. D. Zhou, Magnetic phase diagram of $Ba_3CoSb_2O_9$ as determined by ultrasound velocity measurements, Phys. Rev. B **92**, 014414 (2015).

[51] S. Skanthakumar and J. W. Lynn, Field dependence of the magnetic ordering of Cu in R_2Cu0_4 (R = Nd,Sm), J. Appl. Phys. **73**, 6326 (1993).

[52] S. Skanthakumar, J. W. Lynn, J. L. Peng, and Z. Y. Li, Observation of noncollinear magnetic structure for the Cu spins in Nd_2CuO_4-type systems, Phys. Rev. B **47**, 6173 (1993).

[53] I. W. Sumarlin, J. W. Lynn, T. Chattopadhyay, S. N. Barilo, and D. I. Zhigunov, Dispersion of the magnetic excitations of the Pr ions in Pr_2CuO_4, Physica C Supercond. **219**, 195 (1994).

[54] R. Sachidanandam, T. Yildirim, A. B. Harris, A. Aharony, and O. Entin-Wohlman, Single-ion anisotropy, crystal-field effects, spin reorientation transitions, and spin waves in R_2CuO_4 (R=Nd, Pr, and Sm), Phys. Rev. B **56**, 260 (1997).

[55] B. C. den Hertog and M. J. P. Gingras, Dipolar Interactions and Origin of Spin Ice in Ising Pyrochlore Magnets, Phys. Rev. Lett. **84**, 3430 (2000).

[56] J. A. Paddison, H. S. Ong, J. O. Hamp, P. Mukherjee, X. Bai, M. G. Tucker, N. P. Butch, C. Castelnovo, M. Mourigal, and S. E. Dutton, Emergent order in the kagome Ising magnet $Dy_3Mg_2Sb_3O_{14}$, Nat. Commun. **7**, 13842 (2016).

[57] Z. Dun, X. Bai, J. A. M. Paddison, E. Hollingworth, N. P. Butch, C. D. Cruz, M. B. Stone, T. Hong, F. Demmel, M. Mourigal, and H. Zhou, Quantum Versus Classical Spin Fragmentation in Dipolar Kagome Ice $Ho_3Mg_2Sb_3O_{14}$, Phys. Rev. X **10**, 031069 (2020).

[58] M. Hoffmann and S. Blügel, Systematic derivation of realistic spin models for beyond-Heisenberg solids, Phys. Rev. B **101**, 024418 (2020).